

Theory of traveltimes shifts around compacting reservoirs: 3D solutions for heterogeneous anisotropic media

Rodrigo Felício Fuck¹, Andrey Bakulin², and Ilya Tsvankin¹

ABSTRACT

Time-lapse traveltimes shifts of reflection events recorded above hydrocarbon reservoirs can be used to monitor production-related compaction and pore-pressure changes. Existing methodology, however, is limited to zero-offset rays and cannot be applied to traveltimes shifts measured on prestack seismic data. We give an analytic 3D description of stress-related traveltimes shifts for rays propagating along arbitrary trajectories in heterogeneous anisotropic media. The nonlinear theory of elasticity helps to express the velocity changes in and around the reservoir through the excess stresses associated with reservoir compaction. Because this stress-induced velocity field is both heterogeneous and anisotropic, it should be studied using prestack traveltimes or amplitudes. Then we obtain the traveltimes shifts by first-

order perturbation of traveltimes that accounts not only for the velocity changes but also for 3D deformation of reflectors. The resulting closed-form expression can be used efficiently for numerical modeling of traveltimes shifts and, ultimately, for reconstructing the stress distribution around compacting reservoirs. The analytic results are applied to a 2D model of a compacting rectangular reservoir embedded in an initially homogeneous and isotropic medium. The computed velocity changes around the reservoir are caused primarily by deviatoric stresses and produce a transversely isotropic medium with a variable orientation of the symmetry axis and substantial values of the Thomsen parameters ϵ and δ . The offset dependence of the traveltimes shifts should play a crucial role in estimating the anisotropy parameters and compaction-related deviatoric stress components.

INTRODUCTION

Traveltimes shifts (differences), measured between two or more time-lapse seismic reflection surveys, have become an important tool for dynamic reservoir characterization. Production-related pore-pressure changes and compaction inside the reservoir cause accumulation of stress throughout the section. This excess stress modifies the elastic properties of rocks inside and around the reservoir, and the corresponding velocity changes can be estimated using reflection traveltimes recorded in time-lapse surveys. Analysis of traveltimes shifts can help to map compaction throughout a reservoir, and therefore optimize infill drilling and hydrocarbon production by identifying compartments and pressure cells inside the producing units.

The stress dependence of traveltimes shifts is well understood for vertically propagating waves and horizontal layers (i.e., for zero-offset data). Traveltimes shifts estimated on stacked seismic data from horizontally layered media have been used successfully to delineate

compartments in reservoirs (e.g., Landrø and Stammeijer, 2004; Hatchell and Bourne, 2005). However, this theory breaks down in the presence of dip and cannot be applied to prestack data, as demonstrated by data from South Arne field in the North Sea (Herwanger et al., 2007). Røste et al. (2006) analyzed offset-dependent traveltimes shifts, but their theory is restricted to horizontally layered isotropic media. Herwanger et al. (2007) used nonlinear elasticity to model the offset variation of traveltimes shifts, but they do not present explicit expressions relating shifts to the stress field.

Here we provide an analytic 3D description of traveltimes shifts around a compacting reservoir embedded in a heterogeneous, layered, anisotropic medium. Taking heterogeneity and anisotropy into account is necessary for an adequate physical description of traveltimes shifts. Indeed, the excess stress field created by compaction is anisotropic (in general, it is triaxial) and heterogeneous because the magnitude of stress depends on reservoir geometry and varies spatially around the reservoir.

Manuscript received by the Editor 14 February 2008; revised manuscript received 20 August 2008; published online 17 December 2008.

¹Colorado School of Mines, Center for Wave Phenomena, Golden, Colorado, U.S.A. E-mail: rfuck@dix.mines.edu; ilya@dix.mines.edu.

²Formerly Shell International Exploration and Production Inc., Houston, Texas, U.S.A.; presently WesternGeco, Houston, Texas, U.S.A. E-mail: abakulin@slb.com.

© 2009 Society of Exploration Geophysicists. All rights reserved.

Our analysis of traveltimes shifts in and around a compacting reservoir involves two main steps. We start by expressing the velocity changes through the excess stress and strain fields created by the compaction. Then the first-order perturbation of traveltimes is used to obtain a linearized analytic approximation for the traveltimes shifts.

To describe stress-related velocity changes, we apply the nonlinear theory of elasticity (e.g., [Thurston and Brugger, 1964](#)), which has several advantages over more conventional approaches to model stress-sensitivity of velocity fields. First, it does not rely on a specific micromechanical model, and therefore it is more general than approaches based on stiffening of grain contacts and closing or opening of specific microcrack distributions ([Shapiro and Kaselow, 2005](#)). Second, nonlinear elasticity yields the full stiffness tensor of the deformed medium needed to compute traveltimes and other signatures for arbitrarily anisotropic media.

Third, all possible mechanisms of stress sensitivity are absorbed by a small number of third-order elastic coefficients. For instance, an isotropic third-order strain-sensitivity tensor is defined completely by three parameters. In contrast, fracture models include at least two sets of penny-shaped fractures, with each set defined by three parameters. Fourth, third-order elastic coefficients can be measured directly in laboratory or wellbore experiments (e.g., [Sinha and Plona, 2001](#)), whereas the fracture weaknesses must be inverted from field data ([Sayers, 2006](#)).

The nonlinear theory has been applied successfully to estimate stress-induced anisotropy and the corresponding stress-sensitivity (or strain-sensitivity) tensor in sandstones and shales. Examples include ultrasonic velocity experiments on rock samples ([Johnson and Rasolofosaon, 1996](#); [Sarkar et al., 2003](#); [Prioul et al., 2004](#)) and in-situ stress estimation in boreholes ([Winkler et al., 1998](#); [Sinha and Plona, 2001](#)). Unfortunately, measurements of third-order elastic coefficients (which represent elements of a sixth-rank tensor) for sedimentary rocks are rare, with most existing results obtained for crystals and man-made materials. This is an inherent limitation of our approach, but we expect more data to be available in the near future, in particular because of the straightforward way of measuring third-order coefficients in the laboratory or boreholes. In addition, the results of [Prioul et al. \(2004\)](#) indicate that detailed knowledge of the sixth-order elasticity tensor is not critical, and for most applications in exploration and reservoir geophysics that tensor can be assumed to be isotropic.

We start by describing the variational problem related to the first-order perturbation of traveltimes. Then perturbation theory and nonlinear elasticity are used to express traveltimes shifts in terms of the excess stresses and volumetric strains caused by reservoir compaction. Synthetic tests for a 2D reservoir model confirm that the stress-induced velocity field is anisotropic and illustrate the offset dependence of traveltimes shifts for reflectors above and below the reservoir.

P-WAVE TRAVELTIME SHIFTS FROM FIRST PRINCIPLES

Assuming that reservoir compaction produces only small changes in the traveltimes of seismic waves propagating through the medium, such traveltimes shifts can be expressed through small perturbations of the model parameters. The deformation caused by compaction changes the relative positions of the boundaries between layers, while the extra stress alters the elastic properties. Therefore, travel-

time shifts depend on perturbations of the geometry of the medium interfaces and elastic (stiffness) moduli.

To obtain first-order traveltimes perturbations, we apply Hamilton's principle of least action to traveltimes computed for rays traced in an unperturbed background medium. For simplicity, we consider this background medium to be isotropic, with smoothly varying velocity and density, and restrict the analysis to P-waves. Then the traveltimes shifts δt are described by the following equation well known in classical mechanics (e.g., [Lanczos, 1986](#)):

$$\delta t = \mathbf{p} \cdot \delta \mathbf{x} \Big|_{\tau_1}^{\tau_2} - \int_{\tau_1}^{\tau_2} \Delta \mathcal{H} d\tau, \quad (1)$$

where \mathbf{p} is the slowness vector of the reference ray traced in the background medium, $\delta \mathbf{x}$ is the first-order variation of the position vector of the reference ray in 3D Cartesian coordinates, $\Delta \mathcal{H}$ is the corresponding variation of the system's Hamiltonian, and τ is the integration parameter along the reference ray. The Hamiltonian \mathcal{H} of the system is the scaled eikonal equation, in which the integration parameter τ represents the traveltimes along the reference ray (e.g., [Červený, 2001](#)):

$$\mathcal{H}(\mathbf{x}, \mathbf{p}) = \frac{1}{2} [V^2(\mathbf{x}, \mathbf{p}) p_k p_k - 1] = 0, \quad (2)$$

where $V(\mathbf{x}, \mathbf{p})$ is the phase velocity; summation over repeated indices is implied throughout the paper.

Equation 1 provides important insights into the nature of traveltimes shifts caused by reservoir compaction. First, in the linear approximation the contributions of geometric and velocity changes to traveltimes are independent. Second, the changes of the ray trajectory (i.e., geometric changes) contained in the term $\mathbf{p} \cdot \delta \mathbf{x}$ do not contribute to first-order traveltimes perturbations, unless they occur at the endpoints. Third, the influence of the velocity changes is represented by the perturbed Hamiltonian $\Delta \mathcal{H}$, which should be integrated along the reference ray.

Traveltimes shifts in layered media

Equation 1 is designed for rays traced in smoothly heterogeneous media (Figure 1a). If the medium is stratified, it is necessary to account for deformation of the reflectors that move the reflection/transmission points along the ray. This can be done by dividing the reference ray into segments, applying equation 1 to each of them, and then summing up the results ([Farra and Le Bégat, 1995](#)). For the ray in Figure 1b, equation 1 is applied to segments **SA**, **AB**, **BC**, and **CR** separately, with subsequent summation of the individual contributions. Therefore, extension of equation 1 to layered media accounts for the movement of all N scattering (reflection/transmission) points along the raypath:

$$\delta t^i = (\dot{\mathbf{p}} - \mathbf{p})^i \cdot \delta \mathbf{x}^i \quad (i = 1, 2, \dots, N), \quad (3)$$

where $\dot{\mathbf{p}}$ and \mathbf{p} are the slowness vectors of the incident and scattered (reflected or transmitted) rays, respectively. Note that each scattering point i belongs to two ray segments.

By separating the contribution of the endpoints (δt^e) from that of the scattering points ($i = 1, 2, \dots, N$), equation 1 can be generalized for any number of layers arbitrarily deformed in 3D space:

$$\delta t = \delta t^e + \sum_{i=1}^N \delta t^i - \int_{\tau_1}^{\tau_2} \Delta \mathcal{H} d\tau, \quad (4)$$

where

$$\delta t^e = \mathbf{p} \cdot \delta \mathbf{x} \Big|_{\tau_1}^{\tau_2}, \quad \delta t^i = (\hat{\mathbf{p}} - \mathbf{p}) \cdot \delta \mathbf{x}. \quad (5)$$

Equation 4 can be simplified further by taking Snell's law into consideration. Because the projection of the slowness vector onto the interface is conserved, the only nonzero component of vector $(\hat{\mathbf{p}} - \mathbf{p})$ is that orthogonal to the interfaces. If layer boundaries are horizontal, the traveltimes shifts depend on just the vertical components of the vector $(\hat{\mathbf{p}} - \mathbf{p})$. For interfaces with arbitrary orientation, the unit normal vector (i.e., the vector perpendicular to the interface) at the reflection/transmission point \mathbf{x} is given by the gradient of the unperturbed interface $f(\mathbf{x}) = 0$:

$$\mathbf{N}(\mathbf{x}) = \frac{\nabla f(\mathbf{x})}{|\nabla f(\mathbf{x})|}. \quad (6)$$

To find the component of the vector $(\hat{\mathbf{p}} - \mathbf{p})$ in the direction of $\mathbf{N}(\mathbf{x})$, we use the projection operator $\mathbf{A}(\mathbf{x})$:

$$\mathbf{A} = \frac{\mathbf{N}\mathbf{N}^T}{\mathbf{N}^T\mathbf{N}}. \quad (7)$$

Applying equation 7 to each term $(\hat{\mathbf{p}} - \mathbf{p}) \cdot \delta \mathbf{x}$ in equation 4 gives

$$(\hat{\mathbf{p}} - \mathbf{p}) \delta \mathbf{x}_i = A_{ij} (\hat{\mathbf{p}} - \mathbf{p}) \delta \mathbf{x}_j. \quad (8)$$

Traveltime shifts in heterogeneous anisotropic media

As discussed above, reservoir compaction causes the velocity field around the reservoir to become both heterogeneous and anisotropic. Note that equation 1 involves no assumptions regarding the heterogeneity or anisotropy of the Hamiltonian or its perturbation $\Delta \mathcal{H}$. The generality of equation 1 helps to construct ray-tracing solutions for heterogeneous, arbitrarily anisotropic media (e.g., Jech and Pšenčík, 1989; Chapman and Pratt, 1992; Červený, 2001). The perturbation $\Delta \mathcal{H} = \Delta V/V$ is obtained from equation 2 for the reference ray with the components p_i held constant. Perturbing the Christoffel equation for P-waves leads to the following expression for the term ΔV under the assumption that reference rays are traced in an isotropic medium (Červený, 2001):

$$\Delta \mathcal{H} = \frac{1}{2} \frac{\Delta a_{ijkl}(\mathbf{x}) n_i n_j n_k n_l}{V^2(\mathbf{x})}, \quad (9)$$

where Δa_{ijkl} are perturbations of the density-normalized stiffness coefficients, and n_i are components of the unit slowness vector.

RELATING VELOCITY CHANGES TO EXCESS STRESSES

Equations 4 and 9 provide the basis for analytic description of compaction-induced traveltimes shifts. The next step is to express the density-normalized stiffnesses Δa_{ijkl} in terms of the strains and excess stresses caused by reservoir compaction. As discussed in the introduction, we apply the nonlinear theory of elasticity to describe the stress sensitivity of the stiffness coefficients. The two main assumptions used here are that the strain-sensitivity tensor is isotropic and stress-induced anisotropy is weak.

Nonlinear elasticity

According to Prioul et al. (2004), the effective stiffness coefficients c_{ijkl} of an elastic medium deformed under stress can be written in terms of the predeformation stiffnesses (c_{ijkl}^0) and the deformation-induced changes of the stress (ΔS_{ij}) and strain (Δe_{ij}) tensors:

$$c_{ijkl} = c_{ijkl}^0 + \Delta S_{ik} \delta_{jl} + c_{ijklmn} \Delta e_{mn} + c_{ijpl}^0 \Delta e_{kp} + c_{ipkl}^0 \Delta e_{jp}, \quad (10)$$

where δ_{ij} is Kronecker's symbol, and c_{ijklmn} is a sixth-rank tensor with no more than 56 independent elements (Hearmon, 1953)³. Provided that deformation is small and elastic, equation 10 represents a suitable local linear approximation for the changes in the stiffness elements, similar to a Taylor series expansion around c_{ijkl}^0 . We reduce the number of independent components of c_{ijklmn} to three by assuming that this tensor is isotropic, as suggested by Prioul et al. (2004).

For typical magnitudes of compaction-related stress changes (2–10 MPa inside the reservoir and one-tenth of that outside), equation 10 can be simplified further by dropping relatively small terms. Indeed, laboratory measurements have shown that typically

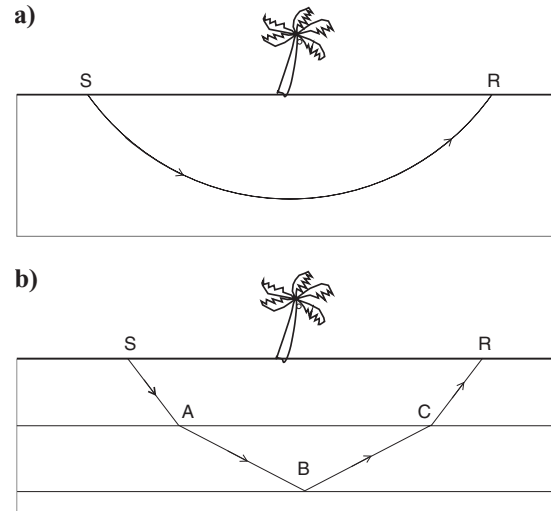


Figure 1. Equation 1 is valid for rays traced in a smoothly heterogeneous medium (a). For layered media (b), it is necessary to account for the movement of reflection (B) and transmission (A, C) points (see equation 4).

³The qualifier “nonlinear” comes from the inclusion of the tensor c_{ijklmn} into Hooke's law (Thurston and Brugger, 1964).

$\Delta S_{ij} \ll c_{ijkl} \ll c_{ijklmn}$ (e.g., Johnson and Rasolofosaon, 1996), which allows us to neglect the terms $\Delta S_{ik} \delta_{jl}$, $c_{ijpl}^0 \Delta e_{kp}$, and $c_{ipkl}^0 \Delta e_{jp}$ in equation 10 (Prioul et al., 2004):

$$c_{ijkl} \approx c_{ijkl}^0 + c_{ijklmn} \Delta e_{mn}. \quad (11)$$

Equation 11 shows that the tensor c_{ijklmn} is a measure of the sensitivity of the stiffnesses c_{ijkl} to deformation. Indeed, the definition of c_{ijklmn} in terms of the strain-energy function W (e.g., Hearmon, 1953) corroborates equation 11:

$$c_{ijklmn} \equiv \frac{\partial^3 W}{\partial e_{ij} \partial e_{kl} \partial e_{mn}} = \frac{\partial c_{ijkl}}{\partial e_{mn}}. \quad (12)$$

If the medium density ρ is assumed to be constant, equation 11 yields the changes in the density-normalized stiffnesses Δa_{ijkl} needed in equation 9:

$$\Delta a_{ijkl} = \rho^{-1} \frac{\partial c_{ijkl}}{\partial e_{mn}} \Delta e_{mn} = \rho^{-1} c_{ijklmn} \Delta e_{mn}. \quad (13)$$

Evaluation of the term $c_{ijklmn} \Delta e_{mn}$ is discussed in Appendix A. In the first-order approximation, we can follow Sarkar et al. (2003) and use linear Hooke's law to relate Δe_{ij} to ΔS_{ij} :

$$\Delta a_{ijkl} = \rho^{-1} c_{ijklmn} (c_{mnpq}^0)^{-1} \Delta S_{pq}. \quad (14)$$

Traveltime shifts resulting from compaction

A concise expression for traveltime shifts can be derived by substituting equation 14 into equation 9 for the perturbation of the Hamiltonian. Using the results of Appendix B (equation B-9), we find:

$$\Delta \mathcal{H} = \frac{1}{2} [B_1 \Delta e_{kk} + B_2 (\mathbf{n}^T \Delta \boldsymbol{\sigma} \mathbf{n})], \quad (15)$$

$$B_1 = \frac{1}{3C_{33}^0} (C_{111} + 2C_{112}), \quad B_2 = 2 \frac{C_{155}}{C_{33}^0 C_{44}^0}, \quad (16)$$

where Δe_{kk} is the trace of the strain tensor, and $\Delta \boldsymbol{\sigma}$ is the tensor of deviatoric stress. The constants C_{111} , C_{112} , and C_{155} are elements of the isotropic sixth-order tensor c_{ijklmn} written in Voigt notation, whereas C_{33}^0 and C_{44}^0 are the stiffnesses of the background isotropic medium. The traveltime shifts given by equation 4 then can be rewritten as

$$\delta t = \underbrace{\delta t^e + \sum_{i=1}^N \delta t^i}_{\text{geom}} - \underbrace{\frac{1}{2} \int_{\tau_1}^{\tau_2} [B_1 \Delta e_{kk} + B_2 (\mathbf{n}^T \Delta \boldsymbol{\sigma} \mathbf{n})] d\tau}_{\text{vel}}, \quad (17)$$

where ‘‘geom’’ and ‘‘vel’’ refer to contributions of the geometric and velocity changes.

Except for the possible influence of tides on offshore 4D surveys, typically the ‘‘geometric’’ term is relatively small. Indeed, for the geometric changes to produce a traveltime shift of at least 1 ms, an unlikely set of conditions must take place: the displacements should be on the order of meters; for layered models, the slowness contrasts cannot be smaller than 10^{-2} s/km; and summation should include from 10 to as many as 100 scattering points. When elastic deformation is caused by depletion, however, displacements throughout the section are on the order of centimeters, consistent with the annual

subsidence rates observed in fields such as Valhall (Herwanger and Horne, 2005). In addition, for layered models, there is little room to increase the number of reflection/transmission points without reducing the slowness contrasts.

According to equation 17, the velocity-related traveltime shifts are given by the arithmetic average of the isotropic ($B_1 \Delta e_{kk}$) and anisotropic ($B_2 \mathbf{n}^T \Delta \boldsymbol{\sigma} \mathbf{n}$) terms computed along the raypath. In our sign convention, negative strains denote contraction, whereas positive strains denote extension. (Likewise, negative stresses imply compression.) This means that the coefficient C_{155} and combination $C_{111} + 2C_{112}$ should be negative. Then, according to equations 15–17, compression leads to increase in velocity, which results in negative traveltime shifts. In contrast, traveltime shifts caused by extension are positive.

To clarify how equation 17 generalizes existing results, in Appendix C it is reduced to the equation for zero-offset data from Hatchell and Bourne (2005). In addition to extending the results of Hatchell and Bourne (2005) to nonzero offsets and dipping reflectors, equation 17 provides useful insight into the meaning of different terms. The result of Hatchell and Bourne (2005) for two-way traveltime shifts has the form

$$\delta t = 2 \int_0^z (1 + R) \frac{\Delta e_{zz}}{V(z)} dz. \quad (18)$$

According to equation 17, the ratio R from equation 18 can be written as

$$\delta t = 2 \int_0^z \left[1 + \frac{1}{2} (R_1 + R_2) \right] \frac{\Delta e_{zz}}{V(z)} dz, \quad (19)$$

where

$$\Delta e_{zz} R_1 = -B_1 \Delta e_{kk}; \quad \Delta e_{zz} R_2 = -B_2 \Delta \sigma_{33}. \quad (20)$$

Hence, the ratio R represents the average of two terms related to the volumetric strain and vertical deviatoric stress changes. If the reservoir thickness is much smaller than the reservoir depth, the volumetric changes are expected to be small. Then the ratio R can be used to estimate $\Delta \sigma_{33}$ using reflectors at or above the reservoir. On the other hand, for reservoirs with comparable depth and thickness, R is likely to reflect both volumetric and deviatoric stress changes.

MODELING OF TRAVELTIME SHIFTS

In this section, we use equation 17 to study the influence of reflector deformation and velocity changes on traveltime shifts. First we obtain an analytic expression for traveltime shifts caused by the movement of reflectors in a simple horizontally layered medium. Then we compute and discuss the spatial distribution of traveltime shifts in shot and common-midpoint (CMP) gathers for a 2D model of a compacting reservoir.

Special case: Reflector deformation in a layered medium

We consider a ray that travels from the surface to the bottom of a model composed of two horizontal isotropic layers. The layers are

assumed to have been deformed uniaxially in the z -direction so that the thickness of layer 1 was increased by δz_1 and that of layer 2 by δz_2 (Figure 2).

To study the influence of geometric changes, velocities in the layers (v_1 and v_2) are kept constant after the deformation. Therefore, the exact one-way traveltimes from the top to the bottom of the model after the deformation can be written as

$$t = \frac{z_1 + \delta z_1}{v_1 \cos \theta_1} + \frac{z_2 + \delta z_2}{v_2 \cos \theta_2}, \quad (21)$$

where θ_1 and θ_2 are the angles between the ray and the vertical in the first and second layers, respectively. Hence, the exact traveltimes difference resulting from the deformation is

$$\Delta t_{\text{ex}} = \frac{\delta z_1}{v_1 \cos \theta_1} + \frac{\delta z_2}{v_2 \cos \theta_2}. \quad (22)$$

Expressing Δt_{ex} in equation 22 in terms of the vertical components $q_i = \cos \theta_i / v_i$ of the slowness vector and the propagation angle θ_i ($i = 1, 2$), we find that

$$\Delta t_{\text{ex}} = \delta z_1 q_1 (1 + \tan^2 \theta_1) + \delta z_2 q_2 (1 + \tan^2 \theta_2). \quad (23)$$

Applying equation 17 to the reference ray traced before the deformation (the ray in Figure 2 with the same takeoff angle θ_1) yields an approximation (Δt_{pert}) for Δt_{ex} :

$$\begin{aligned} \delta t^e &= (\delta z_1 + \delta z_2) q_2, \\ \delta t^i &= \delta z_1 (q_1 - q_2), \\ \Delta t_{\text{pert}} &= \delta t^e + \delta t^i = \delta z_1 q_1 + \delta z_2 q_2. \end{aligned} \quad (24)$$

For propagation angles in the range of 25° – 30° , equations 23 and 24 give similar results because $\tan^2 \theta \ll 1$. In particular, for zero-offset rays ($\theta_1 = \theta_2 = 0$), equation 24 is exact. Note that multiplying equations 23 and 24 by a factor of two yields two-way traveltimes shifts for a reference ray with the source located at position s and receiver at $r = s + 2X$ ($X = z_1 \tan \theta_1 + z_2 \tan \theta_2$) on the surface of the model.

Traveltimes shifts resulting from velocity changes

To illustrate the distribution of traveltimes shifts in prestack data, we applied equation 17 to a 2D model that includes a rectangular reservoir embedded in a homogeneous isotropic half-space (Figure 3).

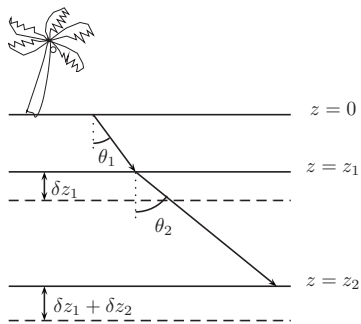


Figure 2. Model of two horizontal layers above a compacting reservoir. The compaction increases the thickness of layer 1 by δz_1 and that of layer 2 by δz_2 . The velocities remain constant after the deformation.

In such a model, traveltimes shifts can be attributed to velocity changes only, because geometric terms will cause shifts not exceeding 10^{-2} ms. The pore-pressure variation occurs only in the reservoir, and the resulting excess stress, strain, and displacement were computed using analytic expressions adapted from Hu (1989). The strain was confined to the incidence plane $[x, z]$, with no deformation in the y -direction ($e_{12} = e_{22} = e_{23} = 0$).

Figure 4 shows the spatial distribution of deviatoric stresses and volumetric strains generated by the pore-pressure drop inside the reservoir. For the plane strain problem treated here, the stress tensor is triaxial, so the 3D stress-induced velocity field has orthorhombic symmetry. The velocity function in the $[x, z]$ -plane, however, can be

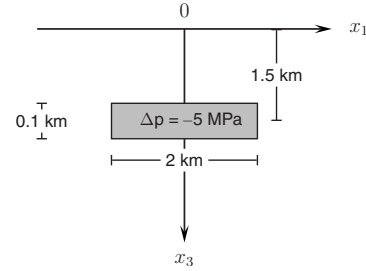


Figure 3. A 2D model of a rectangular reservoir embedded in an isotropic homogeneous medium. The pressure drop inside the reservoir is 5 MPa. The medium parameters are taken from the laboratory results of Sarkar et al. (2003) for Berea sandstone: $V_p = 2.3$ km/s, $V_p/V_s = 1.58$, $\rho = 2.14$ g/cm³, $C_{111} = -13904$ GPa, $C_{112} = 533$ GPa, and $C_{155} = -3609$ GPa. To compute the excess stress, we set the Biot-Willis coefficient α to 0.85 (the closer α is to unity, the more stress is generated by reducing pore pressure in the reservoir). To simulate the static stiffness coefficients, V_p was reduced by 10%, which yields the typical difference between the static and dynamic stiffnesses for well-consolidated rocks with low porosity (Yale and Jamieson, 1994).

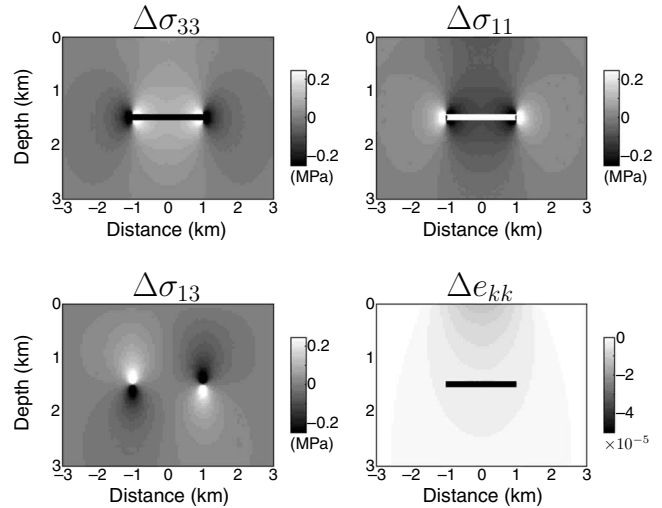


Figure 4. Stress and strain changes for the model from Figure 3 caused by the reservoir compaction. The top row shows changes in the vertical ($\Delta \sigma_{33}$) and horizontal ($\Delta \sigma_{11}$) normal deviatoric stresses. The shear deviatoric stress ($\Delta \sigma_{13}$) and the trace of the strain tensor Δe_{kk} are shown in the second row. Negative values imply compression for stress and contraction (shortening) for strain. Outside the reservoir, $\Delta \sigma_{11} \approx -\Delta \sigma_{33}$. Inside the reservoir, the maximum stress values are $\Delta \sigma_{33} = -2.2$ MPa and $\Delta \sigma_{11} = 1.7$ MPa, whereas the volumetric change is constant: $\Delta e_{kk} = -4.6 \times 10^{-4}$ (the plots were clipped for better visualization).

described by a heterogeneous transversely isotropic (TI) model with a tilted symmetry axis because this vertical plane represents a symmetry plane of the orthorhombic medium.

Using the perturbations of the stiffness coefficients, we computed the stress-related Thomsen parameters ε and δ and rotation angle of the symmetry axis from the vertical (Figure 5). Because the strain-sensitivity tensor and background medium are isotropic, the resulting velocity anisotropy is elliptical ($\varepsilon = \delta$). The absolute δ -values in and near the reservoir reach 0.18, which indicates that the stress-induced anisotropy is nonnegligible even for the relatively small pressure drop (5 MPa) used in the test. The similarity between δ and the normal deviatoric stress components ($\Delta\sigma_{11}$ and $\Delta\sigma_{33}$) is explained by the fact that for our model, $\Delta\sigma_{11} \approx -\Delta\sigma_{33}$. Then, for locations where $\Delta\sigma_{13}$ is small and the symmetry axis is close to vertical, δ is given by (Sarkar et al., 2003)

$$\delta = \frac{C_{155}}{C_{33}^0 C_{44}^0} (\Delta\sigma_{11} - \Delta\sigma_{33}) \approx \frac{2\Delta\sigma_{11} C_{155}}{C_{33}^0 C_{44}^0}. \quad (25)$$

Close to the corners of the reservoir, accumulation of the shear stress $\Delta\sigma_{13}$ causes rotation of the symmetry axis (Figure 5b). Hence, in 3D, the stress-induced anisotropy is described by a tilted orthorhombic model.⁴

Approximate and exact (ray-traced) traveltime shifts are compared in Figure 6. The noticeable discrepancy for reflectors beneath the reservoir is caused by the large velocity change inside the reservoir (as high as 27% for the P-wave vertical velocity). For deep reflectors, the linearized approximation 17 is more accurate in models with lower velocity sensitivity inside the reservoir.

The offset variation of traveltime shifts in Figure 6 is controlled by the spatial distribution of deviatoric stress and volumetric changes as well as by the incidence angle (see equation 17). Because stress-induced velocity changes are concentrated mostly inside and near the reservoir, traveltime shifts are largest for rays that probe the immediate vicinity of the reservoir. We observe two distinct trends for traveltime shifts depending on the CMP location with respect to the reservoir. For common midpoints within the projection of the reservoir onto the surface, traveltime shifts tend to decrease by absolute value with offset (Figures 6 and 7a). In contrast, the magnitude of traveltime shifts for CMP locations outside the reservoir projection generally increases with offset (Figure 7b). Likewise, traveltime shifts in shot gathers become confined mostly to longer offsets as the source is moved away from the reservoir center (Figure 8).

For a fixed CMP or shot location, the offset dependence of traveltime shifts is governed largely by the term $\Delta\sigma_{ij} n_i n_j$ in equation 17. For instance, the reflectors above the reservoir in Figure 7 show an increase rather than a decrease in the magnitude of the shifts for larger offsets.

Ultimately, this variation of traveltime shifts with incidence angle (i.e., with direction \mathbf{n}) might help to estimate components of the deviatoric stress tensor from prestack seismic data. Therefore, it is important to analyze the relative magnitude of traveltime shifts caused by isotropic and anisotropic velocity changes. For the homogeneous and isotropic background model used in the test, volumetric (i.e., isotropic) changes are significant only inside the reservoir (see Figure 4). Thus, traveltime shifts above the reservoir are produced pri-

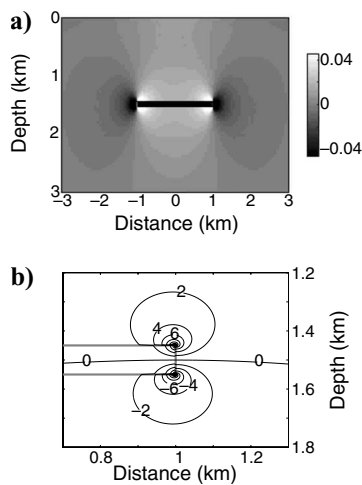


Figure 5. Reservoir compaction makes the medium heterogeneous and anisotropic. (a) The anisotropy parameter $\delta = \varepsilon$ (color scale is clipped); (b) contours of the angle between the symmetry axis and the vertical (positive angle corresponds to clockwise tilt of the axis) near the reservoir right edge (solid gray outline). Inside the reservoir $\delta = -0.18$, whereas the tilt of the symmetry axis at the reservoir corners approaches $\pm 45^\circ$.

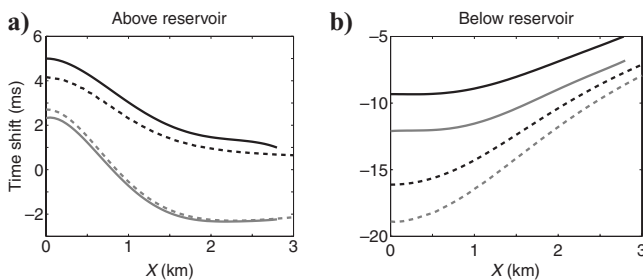


Figure 6. Comparison between traveltime shifts in CMP geometry computed by ray tracing (solid lines) and from equation 17 (dashed). The CMP is located above the center of the reservoir ($x = 0$ km in Figure 3). The depths of imaginary reflectors are (a) 1 km (gray) and 1.45 km (black); (b) 1.55 km (gray) and 2 km (black). For this geometry, $X = 1/2(s - r)$, where s and r denote the source and receiver positions.

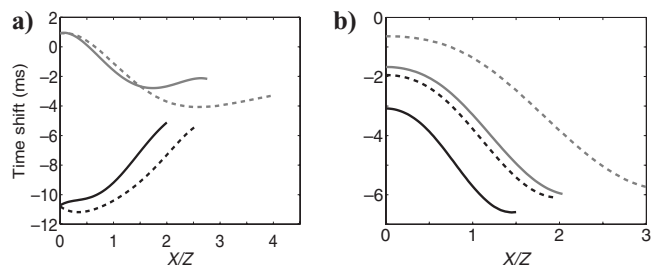


Figure 7. Traveltime shifts in CMP geometry for common midpoints at (a) $x = 1$ km and (b) $x = 2$ km. The gray lines correspond to imaginary reflectors above the reservoir at depths 1 km (dashed) and 1.45 km (solid). The black lines correspond to reflectors below the reservoir at 1.55 km (dashed) and 2 km (solid). Expression X/Z is the ratio of the half-offset and reflector depth, which is equal to $\tan \theta$ for the reference ray.

⁴The medium symmetry can be verified by setting $e_{22} = e_{12} = e_{23} = 0$ in equations A-16–A-33.

marily by deviatoric stress (i.e., anisotropic) changes, whereas volumetric changes make a nonnegligible contribution for reflectors at and below the reservoir level (see Figure 9).

Still, the character of the offset variation of traveltime shifts is controlled largely by the anisotropic terms even for deep reflectors, especially for common midpoints close to the center of the reservoir (Figure 10). For CMP locations inside the reservoir projection onto the surface, the isotropic and anisotropic components of the traveltime shifts have slopes of opposite sign (Figure 10a-d). In contrast, the slopes have the same sign for common midpoints outside the reservoir projection (Figure 10e and f). Therefore, if the volumetric term is neglected in an inversion scheme, deviatoric stress changes reconstructed from traveltime shifts will be underestimated for CMP locations inside the reservoir projection and overestimated for those outside it. The sharp variations of small-offset shifts near the reservoir edges ($x = \pm 1$ km) in Figure 10 are caused by singularities in the analytic solutions for stress used in the modeling.

Figure 11 demonstrates that the vertical stress change ($\Delta\sigma_{33}$) governs small-offset traveltime shifts, whereas contributions of the horizontal and shear stresses gradually increase with offset. Indeed, for our 2D model the term $\Delta\sigma_{ij} n_i n_j$ in equation 17 takes the form

$$\Delta\sigma_{ij} n_i n_j = \Delta\sigma_{33} \cos^2 \theta + 2\Delta\sigma_{13} \cos \theta \sin \theta + \Delta\sigma_{11} \sin^2 \theta, \quad (26)$$

where θ , as before, is the incidence angle. Clearly, the sensitivity of traveltime shifts to the components $\Delta\sigma_{13}$ and $\Delta\sigma_{11}$ increases with offset.

Equation 26 and Figure 11 indicate that, in principle, the horizontal and shear stress changes can be estimated from the offset dependence of traveltime shifts. Reconstruction of the stress components,

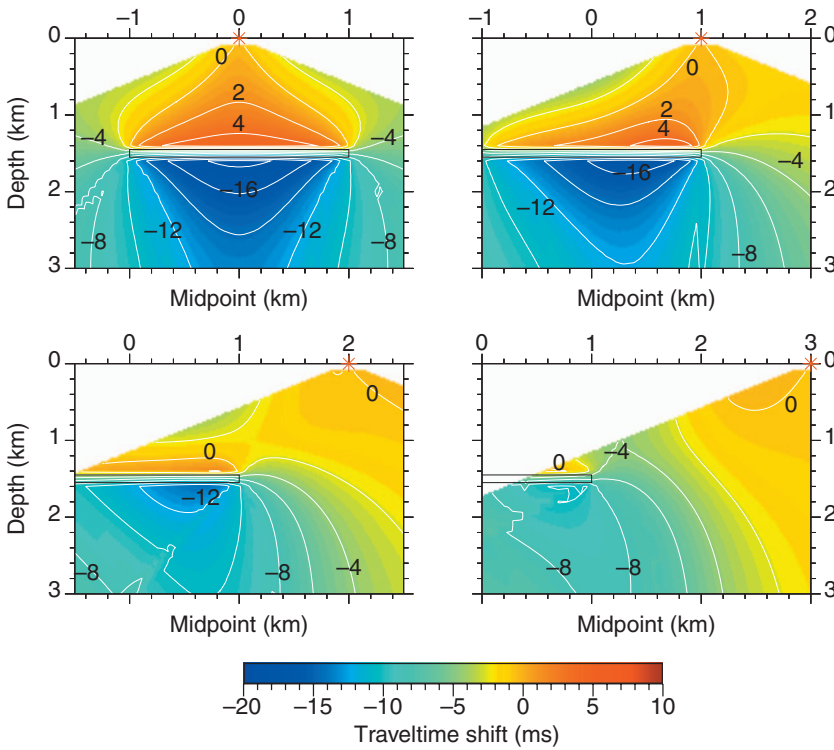


Figure 8. Traveltime shifts for four shot locations (between 0 and 3 km) marked by the asterisk. The shift plotted at each (x, z) point would be recorded at the source-receiver offset $2x$ (i.e., the midpoint is at location x) from an imaginary horizontal interface at depth z . The reservoir is marked by the black rectangle.

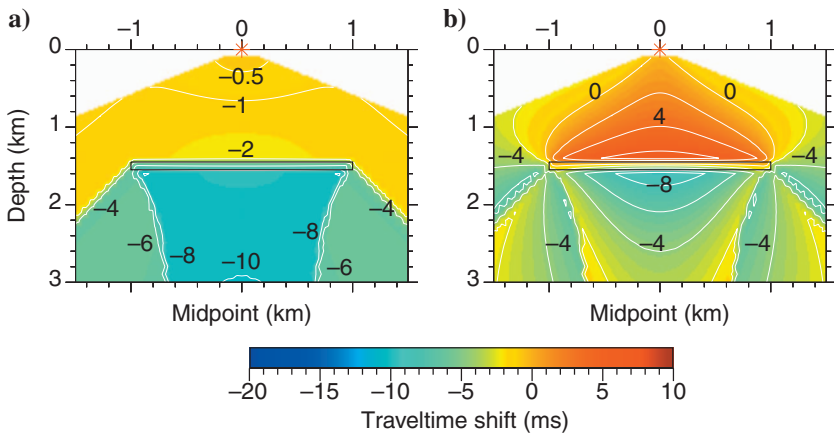


Figure 9. Traveltime shifts for a shot (marked by the asterisk) above the center of the reservoir (same display as in Figure 8). Contributions of the volumetric changes (a) and deviatoric stress changes (b) are computed separately.

however, is complicated by the strong heterogeneity of the excess stress field around the reservoir. As illustrated by Figure 12a, for a relatively shallow reflection event recorded above the center of the reservoir, the slope of the function δt up to relatively long offsets is

governed mostly by $\Delta\sigma_{11}$. However, when the CMP is located above the edge of the reservoir (Figure 12b), the offset variation of traveltime shifts is dominated by $\Delta\sigma_{13}$ with contributions from $\Delta\sigma_{33}$ and $\Delta\sigma_{11}$.

Figure 10. Traveltime shifts in CMP geometry for three midpoints x (each row corresponds to a midpoint) and two reflector depths z . (a) $x = 0$ km, $z = 1.55$ km; (b) $x = 0$ km, $z = 2$ km; (c) $x = 1$ km, $z = 1.55$ km; (d) $x = 1$ km, $z = 2$ km; (e) $x = 2$ km, $z = 1.55$ km; and (f) $x = 2$ km, $z = 2$ km. The total shifts (solid black lines) are plotted along with the shifts resulting from the volumetric changes (dashed gray) and deviatoric stress changes (dashed black).

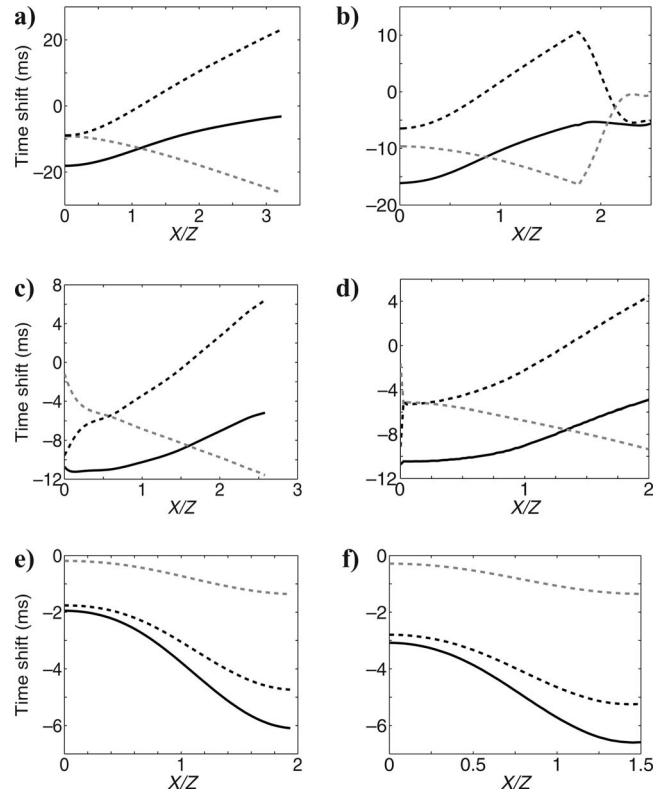
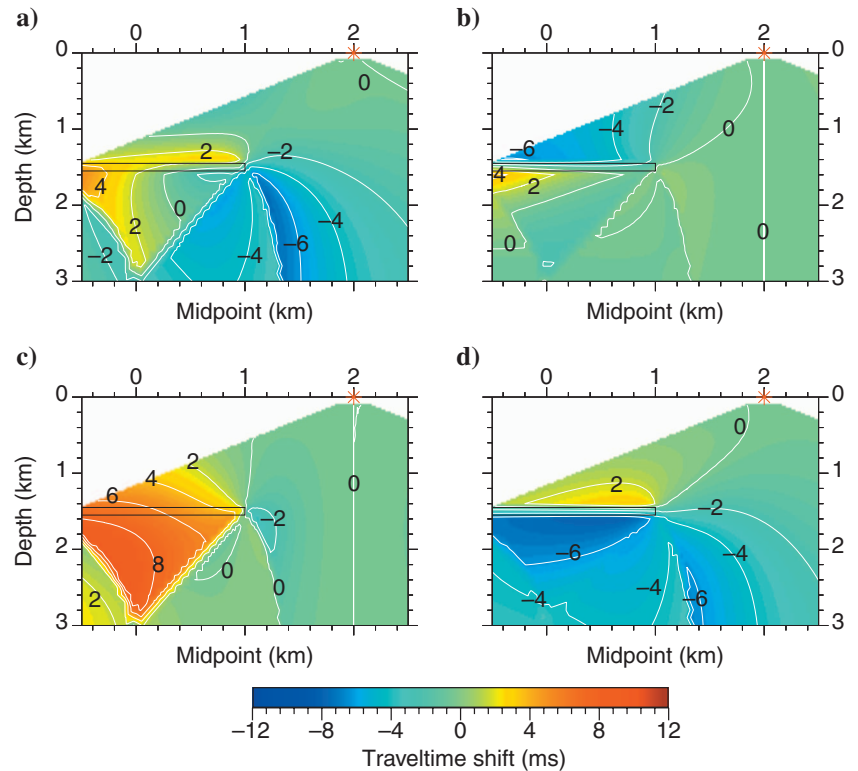


Figure 11. Contributions of the three deviatoric stress components to traveltime shifts for the shot at $x = 2$ km (asterisk) from Figure 8. The shift resulting from (a) the total deviatoric stress change ($\Delta\sigma_{11} + \Delta\sigma_{13} + \Delta\sigma_{33}$); (b) $\Delta\sigma_{11}$; (c) $\Delta\sigma_{13}$; and (d) $\Delta\sigma_{33}$.



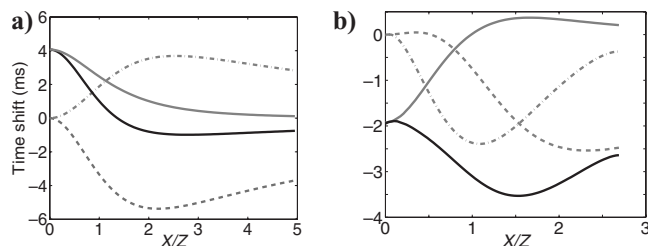


Figure 12. Contributions of the three deviatoric stress components to traveltime shifts in CMP geometry for (a) $x = 0$ km, $z = 1$ km; and (b) $x = 1.1$ km, $z = 1.45$ km. The shifts resulting from the total deviatoric stress change (solid black lines) are plotted along with the contributions of $\Delta\sigma_{11}$ (dashed), $\Delta\sigma_{13}$ (dash-dotted), and $\Delta\sigma_{33}$ (solid gray).

CONCLUSIONS

Our analytic description of compaction-related traveltime shifts is based on three main assumptions. First, a closed-form expression for traveltime shifts was obtained using first-order traveltime perturbations. Anisotropic ray tracing for a 2D model of a compacting reservoir confirms that the first-order approximation reproduces the general behavior of traveltime shifts. The approximate solution produces substantial errors for deep reflectors when the velocity changes inside the reservoir are large (30% or so). However, case studies of compaction-related traveltime shifts suggest that the model likely exaggerates the strain sensitivity inside the reservoir. Second, we used an isotropic sixth-order strain-sensitivity tensor to describe the influence of stress on the stiffness coefficients. Although this assumption limits the stress-induced anisotropic model to the special case of tilted orthorhombic symmetry⁵, it also reduces the number of model parameters and helps to derive concise expressions for traveltime shifts.

Third, deformation was assumed to be purely elastic, which is not always appropriate for velocity changes inside a compacting reservoir (or within a reactivated fault zone outside it) where the contribution of anelastic processes might be substantial. We believe, however, that the physical insight provided by our relatively simple equations justifies neglecting plastic deformation. Also, experimental studies confirm that elastic theory adequately describes a wide range of deformation processes caused by reservoir depletion in various geologic settings.

The main result of our analytic development is equation 17, which generalizes the expressions for zero-offset traveltime shifts and those for offset-dependent traveltime shifts in isotropic media. The simple structure of equation 17 helped us to gain valuable insight into the behavior of compaction-related traveltime shifts in CMP and shot gathers.

Traveltime shifts are caused by two factors — geometric and velocity changes. Analysis of equation 17 indicates that the geometric component of the traveltime shifts typically is at least an order of magnitude smaller than the contribution of the velocity changes. Traveltime shifts resulting from velocity changes could be separated further into two components, one of which is related to volumetric changes and the other to deviatoric stresses. Significant volumetric changes are restricted to the reservoir and to the vicinity of the model surface. The deviatoric stress term, which is related to changes in nonhydrostatic stress, controls the velocity anisotropy of the deformed elastic medium. Equations 16 and 17 also reveal the role of

different components of the strain-sensitivity tensor. In particular, the combination $C_{111} + 2C_{112}$ is responsible for the isotropic P-wave velocity changes, whereas (in agreement with previously published results) C_{155} governs the magnitude of the stress-induced velocity anisotropy.

Although the numerical results are obtained for a simple 2D model, they illustrate several important properties of stress-induced variations in reflection traveltimes. First, traveltime shifts for reflectors at and above the reservoir are associated primarily with the deviatoric stress components (i.e., with stress-induced anisotropy). Because anisotropy parameters should be estimated from offset-dependent traveltimes, it would be highly beneficial to include prestack data in time-lapse analysis.

Second, the magnitude of the anisotropy parameters might be substantial, and the orientation of the symmetry axis rapidly varies in space around the reservoir corners (similar variation also is observed for ellipsoidal reservoir models close to the points of maximum curvature). Third, the modeling helps to understand the complex spatial distribution of traveltime shifts caused by the interplay between the propagation direction and different stress components. On the whole, adding an extra dimension (offset) to time-lapse analysis should help to constrain better the geomechanical changes around depleting blocks and improve interpretation of 4D seismic data.

One of the main practical difficulties in modeling and interpretation of compaction-related traveltime shifts is their dependence on the sixth-order strain-sensitivity tensor. Our analytic results, obtained under the simplifying assumption that this tensor is isotropic, include two independent strain-sensitivity elements. Reliable constraints on these two elements can be provided by laboratory measurements of stress sensitivity of reservoir and overburden rocks similar to those already described in the literature.

Further development of the theory presented here could involve several possible directions. The first is to incorporate second-order phenomena, especially those related to the influence of lithostatic and regional stress fields and of plastic deformation. Then it might be possible to evaluate whether the contributions of compressive and tensile stress changes are indeed asymmetrical. Note that existing measurements of traveltime shifts indicate that velocity is much more sensitive to tensile than to compressive stress. Indeed, velocity changes observed inside reservoirs are relatively small despite the strong compression of reservoir rocks. The second topic for future research is to derive similar equations for traveltime shifts of converted modes and pure shear waves. Time-lapse prestack shear-wave data should provide additional constraints on parameters of the stress field. Third, our analytic results can be extended to incorporate intrinsic anisotropy, while keeping the strain-sensitivity tensor isotropic.

ACKNOWLEDGMENTS

We are grateful to members of the A[nisotropy]-Team of the Center for Wave Phenomena (CWP) at Colorado School of Mines (CSM) for helpful discussions. We also thank the associate editor, Mirko van der Baan, two anonymous reviewers, and Martin Landrø for suggestions, which helped to improve this manuscript. This work was supported by the Consortium Project on Seismic Inverse Methods for Complex Structures at CWP and by the Chemical Sciences,

⁵In each of the symmetry planes, the stress-induced anisotropy is elliptical.

Geosciences, and Biosciences Division of the Office of Basic Energy Sciences, Office of Science, U. S. Department of Energy.

APPENDIX A

ELEMENTS OF THE MATRIX $\Delta C_{\alpha\beta}$

Here, we give a brief derivation of the perturbations of the stiffness coefficients obtained from the equation $\Delta c_{ijkl} = c_{ijklmn} \Delta e_{mn}$. To simplify the summation over repeated indices, we take advantage of the following symmetries of the tensor c_{ijklmn} (e.g., [Thurston and Brugger, 1964](#)):

$$c_{ijklmn} = c_{jiklmn} = c_{ijlkmn} = c_{ijklnm} = c_{klijmn} = c_{mnlkij}. \quad (\text{A-1})$$

These symmetries make it possible to use Voigt notation, which reduces the number of independent elements from 729 to 56. These elements are distributed in $6 \times 6 \times 6$ matrices, and the summation is accomplished by multiplying each cube face by the 6×1 vector formed by the element Δe_{ij} of the excess strain tensor:

$$\Delta C_{\alpha\beta} = C_{\alpha\beta\gamma} \Delta E_{\gamma}, \quad (\text{A-2})$$

where

$$\Delta E_{\gamma} = (\Delta e_{11}, \Delta e_{22}, \Delta e_{33}, 2\Delta e_{23}, 2\Delta e_{13}, 2\Delta e_{12})^T. \quad (\text{A-3})$$

The indices α , β , and γ run from 1 through 6.

Application of equation A-2 is simplified greatly if the $C_{\alpha\beta\gamma}$ matrices are formed by isotropic tensors, because such a tensor includes only 20 nonzero elements ([Hearmon, 1953](#)):

$$C_{111} = C_{222} = C_{333}, \quad (\text{A-4})$$

$$C_{144} = C_{255} = C_{366}, \quad (\text{A-5})$$

$$C_{112} = C_{223} = C_{133} = C_{113} = C_{122} = C_{233}, \quad (\text{A-6})$$

$$C_{155} = C_{244} = C_{344} = C_{166} = C_{266} = C_{355}, \quad (\text{A-7})$$

$$C_{123}, \quad (\text{A-8})$$

$$C_{456}. \quad (\text{A-9})$$

The isotropic symmetry of the sixth-order tensor implies that only three of the components listed above are linearly independent. Following the convention adopted in [Thurston and Brugger \(1964\)](#), nonzero elements $C_{\alpha\beta\gamma}$ for isotropic media can be expressed through linear combinations of three Lamé-type parameters ν_i :

$$C_{111} = \nu_1 + 6\nu_2 + 8\nu_3, \quad (\text{A-10})$$

$$C_{112} = \nu_1 + 2\nu_2, \quad (\text{A-11})$$

$$C_{123} = \nu_1, \quad (\text{A-12})$$

$$C_{144} = \nu_2, \quad (\text{A-13})$$

$$C_{155} = \nu_2 + 2\nu_3, \quad (\text{A-14})$$

$$C_{456} = \nu_3. \quad (\text{A-15})$$

Using the tensor symmetries A-1 and equations A-4–A-9, the perturbations $\Delta C_{\alpha\beta}$ from equation A-2 can be written as

$$\Delta C_{11} = C_{111} \Delta E_1 + C_{112} (\Delta E_2 + \Delta E_3), \quad (\text{A-16})$$

$$\Delta C_{22} = C_{111} \Delta E_2 + C_{112} (\Delta E_1 + \Delta E_3), \quad (\text{A-17})$$

$$\Delta C_{33} = C_{111} \Delta E_3 + C_{112} (\Delta E_1 + \Delta E_2), \quad (\text{A-18})$$

$$\Delta C_{44} = C_{144} \Delta E_1 + C_{155} (\Delta E_2 + \Delta E_3), \quad (\text{A-19})$$

$$\Delta C_{55} = C_{144} \Delta E_2 + C_{155} (\Delta E_1 + \Delta E_3), \quad (\text{A-20})$$

$$\Delta C_{66} = C_{144} \Delta E_3 + C_{155} (\Delta E_1 + \Delta E_2), \quad (\text{A-21})$$

$$\Delta C_{12} = C_{123} \Delta E_3 + C_{112} (\Delta E_1 + \Delta E_2), \quad (\text{A-22})$$

$$\Delta C_{13} = C_{123} \Delta E_2 + C_{112} (\Delta E_1 + \Delta E_3), \quad (\text{A-23})$$

$$\Delta C_{23} = C_{123} \Delta E_1 + C_{112} (\Delta E_2 + \Delta E_3), \quad (\text{A-24})$$

$$\Delta C_{14} = C_{144} \Delta E_4, \quad (\text{A-25})$$

$$\Delta C_{15} = \Delta C_{35} = C_{155} \Delta E_5, \quad (\text{A-26})$$

$$\Delta C_{16} = \Delta C_{26} = C_{155} \Delta E_6, \quad (\text{A-27})$$

$$\Delta C_{24} = \Delta C_{34} = C_{155} \Delta E_4, \quad (\text{A-28})$$

$$\Delta C_{25} = C_{144} \Delta E_5, \quad (\text{A-29})$$

$$\Delta C_{36} = C_{144} \Delta E_6, \quad (\text{A-30})$$

$$\Delta C_{45} = C_{456} \Delta E_6, \quad (\text{A-31})$$

$$\Delta C_{46} = C_{456} \Delta E_5, \quad (\text{A-32})$$

$$\Delta C_{56} = C_{456} \Delta E_4. \quad (\text{A-33})$$

APPENDIX B

PERTURBATION OF THE HAMILTONIAN

To derive the perturbation of the Hamiltonian in equation 9 of the main text, we use equation 14 and assume that the strain-sensitivity tensor is isotropic (see Appendix A). First we evaluate the numerator B of equation 9:

$$B = \Delta a_{ijkl} n_i n_j n_k n_l, \quad (\text{B-1})$$

where Δa_{ijkl} are the density-normalized stiffness perturbations, and \mathbf{n} is the unit slowness vector. Using Voigt notation to replace Δa_{ijkl} by the 6×6 matrix $\Delta A_{\alpha\beta}$ (α and β run from 1 through 6), we find that

$$\begin{aligned}
 B = & \Delta A_{11}n_1^4 + \Delta A_{22}n_2^4 + \Delta A_{33}n_3^4 + 2(\Delta A_{12} \\
 & + 2\Delta A_{66})n_1^2n_2^2 + 2(\Delta A_{13} + 2\Delta A_{55})n_1^2n_3^2 \\
 & + 2(\Delta A_{23} + 2\Delta A_{44})n_2^2n_3^2 + 4(\Delta A_{16}n_1^2 \\
 & + \Delta A_{26}n_2^2)n_1n_2 + 4(\Delta A_{15}n_1^2 + \Delta A_{35}n_3^2)n_1n_3 \\
 & + 4(\Delta A_{24}n_2^2 + \Delta A_{34}n_3^2)n_2n_3 + 4(\Delta A_{14} \\
 & + 2\Delta A_{56})n_1^2n_2n_3 + 4(\Delta A_{25} + 2\Delta A_{46})n_1n_2^2n_3 \\
 & + 4(\Delta A_{36} + 2\Delta A_{45})n_1n_2n_3^2. \quad (\text{B-2})
 \end{aligned}$$

Note that $\Delta A_{\alpha\beta} = \rho^{-1}\Delta C_{\alpha\beta}$, where $\Delta C_{\alpha\beta}$ are given by equations A-16–A-33. Substituting equations A-16–A-33 into equation B-2 and taking into consideration equations A-10–A-15 leads to

$$\begin{aligned}
 \rho B = & [C_{111}\Delta E_1 + C_{112}(\Delta E_2 + \Delta E_3)]n_1^4 + [C_{111}\Delta E_2 \\
 & + C_{112}(\Delta E_1 + \Delta E_3)]n_2^4 + [C_{112}(\Delta E_1 + \Delta E_2) \\
 & + C_{111}\Delta E_3]n_3^4 + 2[C_{112}\Delta E_3 + (C_{112} + 2C_{155})(\Delta E_1 \\
 & + \Delta E_2)]n_1^2n_2^2 + 2[C_{112}\Delta E_2 + (C_{112} + 2C_{155})(\Delta E_1 \\
 & + \Delta E_3)]n_1^2n_3^2 + 2[C_{112}\Delta E_1 + (C_{112} + 2C_{155})(\Delta E_2 \\
 & + \Delta E_3)]n_2^2n_3^2 + 4C_{155}n_1n_2n_3(\Delta E_4n_1 + \Delta E_5n_2 \\
 & + \Delta E_6n_3) + 4C_{155}[\Delta E_6n_1n_2(n_1^2 + n_2^2) \\
 & + \Delta E_5n_1n_3(n_1^2 + n_3^2) + \Delta E_4n_2n_3(n_2^2 + n_3^2)]. \quad (\text{B-3})
 \end{aligned}$$

Combining the terms containing C_{111} , C_{112} , and C_{155} in equation B-3 yields

$$\begin{aligned}
 \rho B = & (C_{111} - C_{112})(\Delta E_1n_1^4 + \Delta E_2n_2^4 + \Delta E_3n_3^4) \\
 & + C_{112}e_{kk} + 4C_{155}[\Delta E_1(n_1^2 - n_1^4) + \Delta E_2(n_2^2 - n_2^4) \\
 & + \Delta E_3(n_3^2 - n_3^4) + \Delta E_6n_1n_2 + \Delta E_5n_1n_3 \\
 & + \Delta E_4n_2n_3], \quad (\text{B-4})
 \end{aligned}$$

where Δe_{kk} is the trace of the excess strain tensor $\Delta e_{ij} = \Delta E_{ij}$.

It follows from equations A-10–A-15 that $C_{111} - C_{112} = 4C_{155}$, which allows us to obtain B as

$$\begin{aligned}
 \rho B = & C_{112}\Delta e_{kk} + 4C_{155}(\Delta E_1n_1^2 + \Delta E_6n_1n_2 + \Delta E_2n_2^2 \\
 & + \Delta E_5n_1n_3 + \Delta E_4n_2n_3 + \Delta E_3n_3^2). \quad (\text{B-5})
 \end{aligned}$$

In tensor notation, equation B-5 becomes

$$\rho B = C_{112}\Delta e_{kk} + 4C_{155}\Delta e_{ij}n_in_j. \quad (\text{B-6})$$

The contribution of the quadratic form $\Delta e_{ij}n_in_j$ to the stiffness perturbations in equation B-6 causes the resulting velocity anisotropy to be elliptical.

Another interesting property of equation B-6 is that B is composed of two terms, one of which is controlled by the volumetric changes (i.e., by Δe_{kk}). The strain tensor Δe_{ij} can be represented through its deviatoric ($\Delta \varepsilon_{ij}$) and dilational (Δe_{kk}) components as

$$\Delta e_{ij} = \Delta \varepsilon_{ij} + \frac{1}{3}\Delta e_{kk}\delta_{ij}, \quad (\text{B-7})$$

and equation B-6 takes the form

$$\rho B = \frac{1}{3}(3C_{112} + 4C_{155})\Delta e_{kk} + 4C_{155}\Delta \varepsilon_{ij}n_in_j. \quad (\text{B-8})$$

Using equations A-10–A-15, we find that $3C_{112} + 4C_{155} = C_{111} + 2C_{112}$. Linear Hooke's law helps to express the deviatoric strain through the deviatoric stress as $\Delta \varepsilon_{ij} = \Delta \sigma_{ij}/(2C_{44})$, which leads to the following expression for the term B :

$$\rho B = \frac{1}{3}(C_{111} + 2C_{112})\Delta e_{kk} + 2\frac{C_{155}}{C_{44}}\Delta \sigma_{ij}n_in_j. \quad (\text{B-9})$$

Equation B-9 represents B as the sum of the contributions of the volumetric changes Δe_{kk} and deviatoric stress changes $\Delta \sigma_{ij}$.

APPENDIX C

COMPARISON WITH EQUATIONS FOR ZERO-OFFSET DATA

Here we compare our equation 17 with the equation of Hatchell and Bourne (2005) for zero-offset traveltimes shifts. We consider zero-offset rays reflected from a horizontal interface in an isotropic homogeneous background medium. In addition, displacements are assumed to be vertical. Therefore, the only nonzero components of the slowness and displacement vectors in equation 17 are p_3 and δx_3 :

$$\delta t = p_3u_3\Big|_{\tau_1}^{\tau_2} - \int_{\tau_2}^{\tau_1} \frac{\Delta V}{V} d\tau, \quad (\text{C-1})$$

where $\delta x_3 = u_3$. Bringing the endpoint contributions under the integral, we obtain

$$\delta t = \int_{\tau_1}^{\tau_2} \left[\frac{d(p_3u_3)}{d\tau} - \frac{\Delta V}{V} \right] d\tau. \quad (\text{C-2})$$

Expanding the derivative in the integrand and changing variables ($d\tau = dz/V$) yields the two-way traveltimes shift:

$$\delta t = 2 \int_0^Z \left[Vp_3 \frac{du_3}{dz} + Vu_3 \frac{dp_3}{dz} - \frac{\Delta V}{V} \right] \frac{dz}{V}. \quad (\text{C-3})$$

The integration is carried out from the surface ($z = 0$) to the reflector depth Z . From the eikonal equation, it follows that $p_3 = 1/V$, and

$$\delta t = 2 \int_0^Z \left[\frac{du_3}{dz} + Vu_3 \frac{dp_3}{dz} - \frac{\Delta V}{V} \right] \frac{dz}{V}. \quad (\text{C-4})$$

Because the reference ray is traced in a homogeneous medium, $dp_3/dz = 0$. In addition, according to the definition of the strain tensor, $\Delta e_{zz} = du_3/dz$. Hence,

$$\delta t = 2 \int_0^Z \left[\Delta e_{zz} - \frac{\Delta V}{V} \right] \frac{dz}{V}. \quad (\text{C-5})$$

Equation C-5 is equivalent to the zero-offset result of Hatchell and Bourne (2005), who rewrite δt as follows:

$$\delta t = 2 \int_0^z (1 + R) \frac{\Delta e_{zz}}{V} dz, \quad (\text{C-6})$$

where

$$R = - \frac{\Delta V}{V} \frac{1}{\Delta e_{zz}}. \quad (\text{C-7})$$

The equivalence of equations C-5 and C-6 confirms that equation 17 represents a generalization of previously published results.

REFERENCES

- Červený, V., 2001, *Seismic ray theory*: Cambridge University Press.
- Chapman, C. H., and R. G. Pratt, 1992, Traveltime tomography in anisotropic media I— Theory: *Geophysical Journal International*, **109**, 1–19.
- Farra, V., and S. Le Bégat, 1995, Sensitivity of qP-wave traveltime and polarization vectors to heterogeneity, anisotropy and interfaces: *Geophysical Journal International*, **121**, 371–384.
- Hatchell, P., and S. Bourne, 2005, Rocks under strain: Strain-induced time-lapse time-shifts are observed for depleting reservoirs: *The Leading Edge*, **24**, 1222–1225.
- Hearmon, R. F. S., 1953, Third-order elastic coefficients: *Acta Crystallographica*, **6**, 331–340.
- Herwanger, J., and S. Horne, 2005, Predicting time-lapse stress effects in seismic data: *The Leading Edge*, **24**, 1234–1242.
- Herwanger, J., E. Palmer, and C. R. Schjøtt, 2007, Anisotropic velocity changes in seismic time-lapse data: 77th Annual International Meeting, SEG, Expanded Abstracts, 2883–2887.
- Hu, S. M., 1989, Stress from a parallelepipedic thermal inclusion in a semi-space: *Journal of Applied Physics*, **66**, 2741–2743.
- Jech, J., and I. Pšenčík, 1989, First-order perturbation method for anisotropic media: *Geophysical Journal International*, **99**, 369–379.
- Johnson, P. A., and P. N. J. Rasolofosaon, 1996, Nonlinear elasticity and stress-induced anisotropy in rock: *Journal of Geophysical Research*, **101**, 3113–3124.
- Lanczos, C., 1986, *Variational principles of mechanics*, 4th ed.: Dover Publications Inc.
- Landrø, M., and J. Stammeijer, 2004, Quantitative estimation of compaction and velocity changes using 4D impedance and traveltime changes: *Geophysics*, **69**, 949–957.
- Priou, R., A. Bakulin, and V. Bakulin, 2004, Nonlinear rock physics model for estimation of 3D subsurface stress in anisotropic formations: Theory and laboratory verification: *Geophysics*, **69**, 415–425.
- Røste, T., A. Stovas, and M. Landrø, 2006, Estimation of layer thickness and velocity changes using 4D prestack seismic data: *Geophysics*, **71**, no. 6, S219–S234.
- Sarkar, D., A. Bakulin, and R. L. Kranz, 2003, Anisotropic inversion of seismic data for stressed media: Theory and a physical modeling study on Berea sandstone: *Geophysics*, **68**, 690–704.
- Sayers, C. M., 2006, Sensitivity of time-lapse seismic to reservoir stress path: *Geophysical Prospecting*, **54**, 369–380.
- Shapiro, S. A., and A. Kaselow, 2005, Porosity and elastic anisotropy of rocks under tectonic stress and pore-pressure changes: *Geophysics*, **70**, no. 5, N27–N38.
- Sinha, B. K., and T. J. Plona, 2001, Wave propagation in rocks with elastic-plastic deformations: *Geophysics*, **66**, 772–785.
- Thurston, R. N., and K. Brugger, 1964, Third-order elastic constants and the velocity of small amplitude elastic waves in homogeneously stressed media: *Physical Review*, **133**, no. 6A, A1604–A1610.
- Winkler, K. W., B. K. Sinha, and T. J. Plona, 1998, Effects of borehole stress concentrations on dipole anisotropy measurements: *Geophysics*, **63**, 11–17.
- Yale, D. P., and W. H. Jamieson, Jr., 1994, Static and dynamic mechanical properties of carbonates, in P. P. Nelson and S. E. Laubach, eds., *Rock mechanics models and measurements challenges from industry*. Proceedings of the 1st North American Rock Mechanics Symposium, 463–471. Balkema.